Flow Control Effects on Length Scales Over a Turret

Marlyn Y. Andino and Mark N. Glauser
Syracuse University,
Mechanical and Aerospace Engineering

Abstract
Turbulence has an adverse effect on aero-optic applications when present in separated and inviscid flows, boundary and shear layers. A study of the flow physics around a cylindrical turret with the application of open-loop control has been performed. The evaluation of flow control performance is accomplished by analyzing the changes in the turbulent flow time/length scales across the turret surface for three cases: baseline, modulated sine wave and pure sine wave. Simultaneous velocity and unsteady pressure measurements were acquired at a Reynolds number of 300,000 based on turret's diameter. Turbulence intensity results present reduction of 20% on the u' for the actuated cases. Results of the autocorrelations of the unsteady pressure sensors exhibit a more organized, almost periodic behavior. Flow control demonstrates the ability to organize the flow structures moving the flow towards homogeneity. Even when the measurements performed are not direct measures of the aero-optics, literature suggest that there is a strong relationship between them and the optical quality of the flow. Results are encouraging from the adaptive optics point of view. The flow control is able to "organize" the structures in the shear layer and possibly simplify the application of adaptive optics.

I. INTRODUCTION

The performance of a laser beam projected through a turbulent flow field is diminished by its adverse effects. The presence of turbulence in separated and inviscid flows, boundary and shear layers results in energy distortion of the laser beam. Density fluctuations across the beam aperture causes variation in the index of refraction resulting in attenuation of its intensity. Work done by K. Gilbert (1982) shows optical disturbances caused by shear layers and classifies this as aero-optics problem. Driven by this motivation researchers have applied adaptive-optic systems to attenuate these losses. Recent investigations[2–4] have shown that adaptive-optics methods lessen the atmospheric effects but are incapable to reduce the aerooptical problems because of its spatial and temporal bandwidths. Other investigations[5] have include passive control devices that presented an improvement in the optical propagation environment.

There is potential for the development of a robust dynamical model for flow control around the laser head. Shear layers and separated flows are receptive to external excitation. Similar responsiveness was also found for aero-optics problem making suitable the use of flow control.[5–6] Furthermore, results shown by Andino et. al. (2009) demonstrate that using pressure-based simple proportional closed-loop control there was reduction in the time integral scales and the flow was driven towards homogeneity.

One of our objectives is to reach broad understanding of the flow characteristics and their response to the control input. Our ultimate goal is to understand the flow structures dynamics that are originated by the flow separation over the turret's aperture to develop a dynamical model for flow control. In this work we explore the effects of the interactions between the actuators and the flow on the pressure distribution over the turret. This work focuses only on the turbulent flow physics with and without control. The experiments were performed using a 3D bluffbody with a Reynolds number of 300,000 based on turret diameter and free-stream velocity. An actuation system containing 22 piezo-electric disks was implemented for flow control purposes. Standard Particle Image Velocimetry, (PIV), and simultaneously sampled surface pressure measurements were implemented to capture the behavior of the flow field over our bluffbody. Measurements were obtained for three cases: baseline and two actuation frequencies. Velocity results have shown that actuation used has a positive effect on reducing the turbulence intensity observed at the center plane of the model.

II. EXPERIMENTAL SETUP

A. Wind tunnel and test model

A set of experiments was conducted at Syracuse University in a Gottingen-type, recirculating, subsonic wind tunnel with a variable speed from 2 to 66 *m/s*. The test section is 0.61 $m \times 0.61\ m \times 2.44\ m$ made of plexiglass that gives full optical access. All turret tests were performed at 30 *m/s* corresponding to a Reynolds number of 300,000, based on turret's diameter. Figure 1(a) provides an overview of the turret configuration used for the tests.

The test model consists of a hemisphere-on-cylindrical base, as shown in figure 1(b). The hemisphere is 15.24 *cm* in diameter with a 7.11 *cm* diameter flat aperture at the top of the hemisphere. The aperture is set to have a boresight angle of 120 degrees with respect to the incoming flow, facing downstream. The cylindrical base is 10.16 *cm* high and diameter of 15.24 *cm*. The base of the model rests on a 6061 aluminum alloy splitter plate that is 38.1 *cm* long, 30.48 *cm* wide and 1.27 *cm* thick. This plate allows the angle of attack to be varied with a dynamic pitching system that was constructed for the wind tunnel. For this reason the model was placed parallel to one of the tunnel side-walls. This configuration allowed the placement of the PIV cameras underneath the test section to capture the velocity measurement plane.

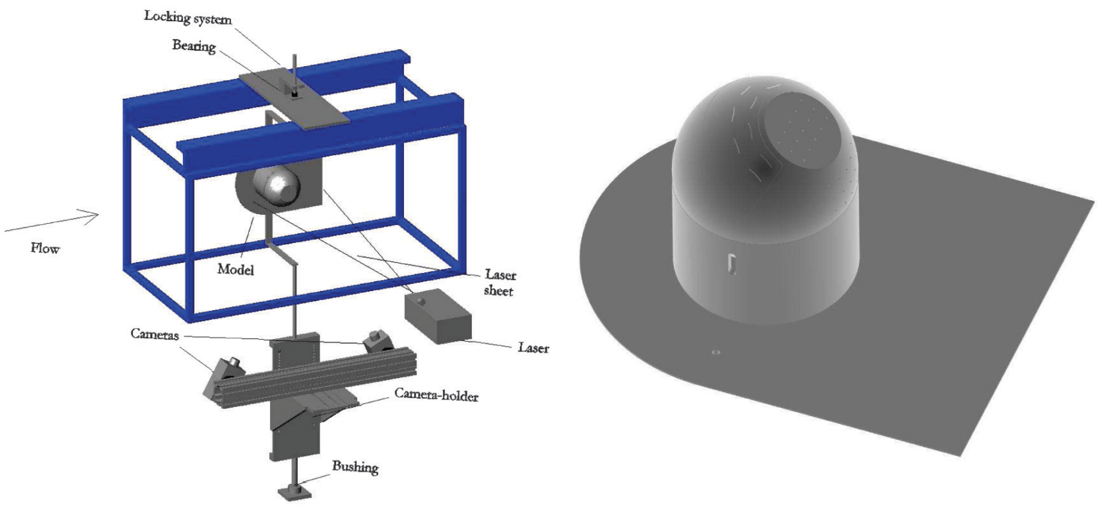

(a) Overall view of cylindrical turret setup. (b) Turret configuration.

Figure 1. Cylindrical turret model.

The actuation system that holds eleven small oscillatory jets in a double-row array is upstream of the leading edge of the aperture radially distributed forming a 180° angle. The actuation bank for the turret was designed in a modular housing as shown in figure 2(a). The synthetic jets[8–9] utilize two ceramic piezo-electric diaphragms sealed into a cavity with only a thin slot, of 0.5 mm wide and 15.24 mm long, to move the air through. The thickness of the cavity is about 2 mm giving a volume of $1.14 \times 10^{-6}\ m^3$. The cavity of the synthetic jets was designed using the Helmholtz resonator principle by setting the resonance frequency of the diaphragm equal to the Helmholtz frequency. The jets' exit is oriented at 30 degrees with respect to the surface of the hemisphere[10] which makes it almost tangent to the flow. The diaphragms are Omega Piezo Technologies, model OPT-BD-27T-2.6A1, as shown in figure 2(b), with a diameter of 27 mm and a resonant frequency of 2.6±0.4 *kHz*. A calibration of the actuation system was performed by measuring the exit velocity of the synthetic jets at various actuation frequencies and amplitudes using a hot wire system. Using results obtained from calibration, two frequencies were selected to drive the actuators and obtain a uniform exit velocity from the actuation bank these are 2.4 *kHz* and 2.2 *kHz*. An average velocity of 50 *m/s* was found at these frequencies at 1 mm downstream of the orifice. The sphere, cylinder and actuation bank were built using stereolithography. This three dimensional printing technology facilitates the creation of a solid, durable and strong plastic prototype using a water resistant resin, *WaterShed* 11120.

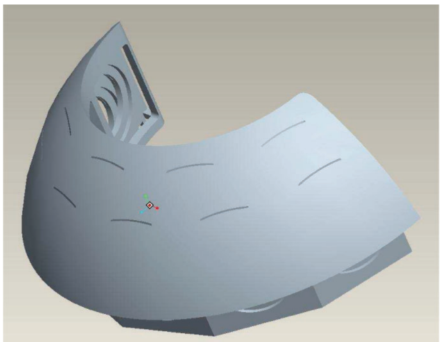

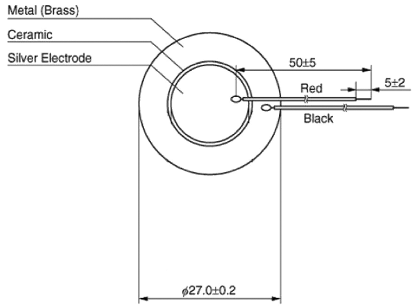

(a) (b)

Figure 2. (a) Actuation bank located by the leading edge of cylindrical turret and (b) Ceramic piezo-electric actuator disk of 27*mm*.

B. Instrumentation and data acquisition system

Dynamic surface pressure measurements were taken simultaneously with velocity using 30 *ICP*® PCB Piezoelectronics sensors, model 103B01, distributed along the surface of the model. On the flat aperture 15 sensors were placed with a 1.27 *cm* spacing between them that forms three rows containing five sensors per row. Another 15 sensors were placed past the trailing edge of the aperture with the same spacing in the cross-stream direction, and placed at 10° between each row in the free-stream direction. Figure 3(a) presents a visual on the distribution of the pressure transducers and table 1 shows their location with respect to the coordinate system. These transducers have a measurement range of 22.9 *kPa*, a resolution of 0.138 *Pa* and a bandwidth of 5 *Hz*–13 *kHz*. The sensors are placed 0.16 *cm* underneath the surface with an adhesive mounting ring of 0.635 mm in thickness and the diameter of the orifice for each transducer is 0.16 *cm*. The calibration for the pressure sensors that provides the sensitivity values was done by the manufacturer.

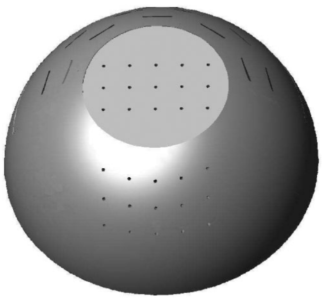

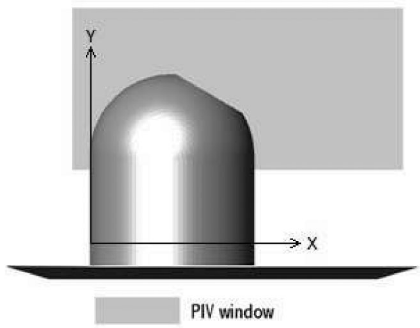

(a) (b)

Figure 3. (a) Pressure sensors distribution and (b) measurement window.

Table 1. Pressure sensors location per measurement plane.

z (cm)	Sensors					
-2.54	1	6	11	16	21	26
-1.27	2	7	12	17	22	27
0	3	8	13	18	23	28
1.27	4	9	14	19	24	29
2.54	5	10	15	20	25	30

A standard Particle Image Velocimetry system, from *Dantec Dynamics*, was used to acquire 2-component velocity vector maps. This system consists of a double pulsed New Wave Research 200 *mJ* Nd:YAG laser with an optical laser sheet generator and two *HiSense* 8 – *bit* resolution CCD cameras.

Two cameras were used to produce a bigger measurement window as shown in figure 3(b). The flow was seeded using olive oil and a TSI Laskin Nozzle generating mean particles sizes of the order of 1 – 10 μm. The particles were injected into the flow stream prior the experiments to assure uniform distribution.

An ensemble of 2000 velocity snapshots was acquired for each of the cases studied. These snapshots are considered to be statistically independent based on the time interval between them. As mentioned previously, the PIV system captured the snapshots at a sampling rate of 3 *Hz*. This corresponds to 333 ms between them, which is larger than the double of the integral time scales for these tests.

Fluctuating surface pressure and PIV trigger signals were recorded simultaneously at 10 *kHz* with a *National Instruments* PXI-8175 with an 866 *MHz* embedded controller, 24 bit high-resolution A/D converters and anti-aliasing filters. These signals were connected to four SCXI-1531 modules of eight-channel ICP® accelerometer in multiplex mode that assure simultaneous sample and hold to preserve phase information. The modules also provide an excitation current of 4 *mA* to the pressure transducers. For the actuation system, six A-303 *AALab Systems* piezo amplifiers were employed. These provided a gain of 15 to the voltage sent from the *National Instruments* PXI-8175 using a D/A PXI-6713 converter module with an signal amplitude of 3 resulting in about 45 *V* peak-to-peak.

III. RESULTS

Velocity flow field and surface pressure measurements are presented here for this experiment. Measurements were acquired for a boresight angle of 120 degrees and a freestream velocity of 30 *m/s*.

A. Velocity measurements

The main objective of this experiment is to evaluate the flow control system's authority. The control objective was to reduce turbulent fluctuations for both velocity and surface pressure as well as the integral scales. In these tests three cases were studied for open-loop: baseline, modulated sine wave, (MSW), and pure sine wave, (PSW), figures 4(a) and 4(b) present the excitation signal for the actuated cases. In the first actuated case, the piezos were modulated at a dimensionless frequency, f^+, of 1 and in the second case the actuation frequency was set at the natural frequency of the piezo-electric disks ($f^+ = 8$). The dimensionless frequency is calculated using equation 1.

$$f^+ = f\frac{x_s}{U_\infty} \tag{1}$$

In equation 1, f is the frequency of modulation of the input signal, x_s is the length of separation over the test model and U_∞ is the free-stream velocity. For this model, we consider that the length of separation started at the leading edge of the aperture and extended to the back of the aperture, this being 11.18 *cm*. Even when the separation is three dimensional we took this length from the center plane. This provides the largest separation over the body. The average momentum coefficient for this test model produced per synthetic jet was 1.7×10^{-3}. This quantity was calculated using the following equation:

$$C_\mu = \frac{\left(\rho A u2\right) jet}{\left(\frac{1}{2}\rho A U2\right)_\infty} \tag{2}$$

where ρ is the density of air, A_{jet} is the area of the jet's exit, A_∞ is the frontal area of the turret, and u_{jet} is the synthetic jet average velocity.

The center plane was selected as the study plane for the results presented here. The instantaneous $\tilde{u}$, $\tilde{v}$ velocity snapshot shown in figure 5(a) demonstrates a few vortices that are produced at the leading edge of the aperture and travel along the separated region. The flow is massively separated and highly three dimensional. The area of the aperture in the figure is located from $x/d = 0.5$ to $x/d = 1$. We can see that the separated flow interferes in the path of the wavefront. As discussed in the literature the separated flow can cause severe optical degradations.

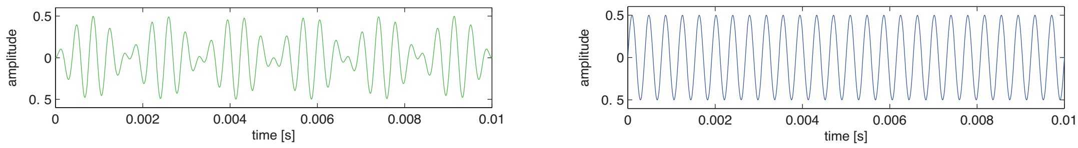

(a) Modulated sine wave (b) Pure sine wave

Figure 4. Excitation input signals for open-loop flow control of the low Reynolds number tests.

A comparison of the instantaneous $\tilde{u}$, $\tilde{v}$ velocity field of the baseline with the actuated cases is done to demonstrate the flow control effect. For the baseline case, figure 5(a) shows the instantaneous $\tilde{u}$, $\tilde{v}$ velocity field for the baseline and the two actuated cases. The formation of a wake is perceived in all three cases. Vortices develop from the leading edge of the aperture and travel along the separated region. A difference present is that for the actuated cases, figures 5(b) and 5(c), the size of the vortices appear to be smaller than for the baseline case. Also, they seem to present a regularization on the vortices that develop for the actuated cases. No major conclusions about the control can be made from the instantaneous velocity field alone. For this reason we follow the analysis and look at the velocity's second moments (u', v').

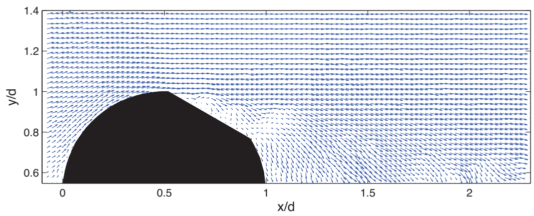

(a) Baseline

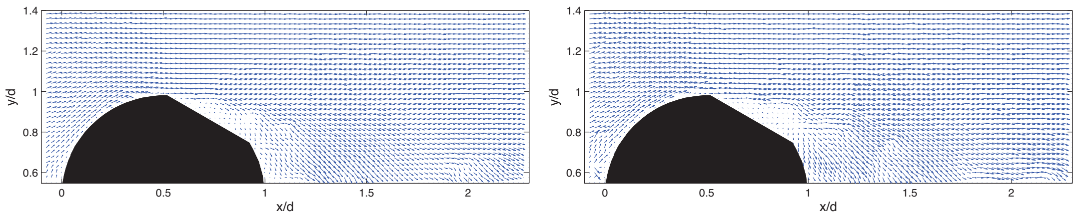

(b) Modulated sine wave, $f^+ = 1$ (c) Pure sine wave, $f^+ = 8$

Figure 5. Instantaneous $\tilde{u}$; $\tilde{v}$ velocity flow field for all cases studied.

A single snapshot can not provide us with a complete description of the flow, therefore we take a look at the mean flow (U, V) and the u', v' velocity fields. These quantities are computed with an ensemble average of 2000 snapshots acquired with the PIV system. The second moment was examined to evaluate the control's effect. Figure 6(a) presents the local normalized turbulence intensity of the streamwise velocity component, $\tilde{u}$. Over the separation area, the turbulence intensity ranges from 10 to 30%. Also in this figure we can see the shear layer that develops with an approximated thickness between 1.52 to 2.54 *cm* across the aperture. The flow field demonstrates a maximum turbulence intensity of 30%, that indicates a high level of turbulence in the area of separation. This maximum is located over the first half of the aperture, which corresponds to 3.56 *cm*. Figure 6(b) presents the turbulence intensity for the cross-stream velocity component, $\tilde{v}$. It is interesting to notice that there is a high turbulence intensity towards the base of the model. This can be attributed to the horseshoe vortex that develops at the base of the model, as presented by Woszildo et. al (2009). The turbulence intensity in that area is of the same order as the one present over the aperture. Large velocity fluctuations are clearly behind the whole model. Results show that the normalized turbulence intensities are reduced with the application of open loop control, shown on figure 6. Specifically in figures 6(c) and 6(e), a reduction of the maximum u' values of 20% is perceived between both of the actuated cases when comparing them to the baseline case shown in figure 6(a). The area with the maximum turbulence intensity also shifts slightly towards the downstream side of the aperture, an indication of delayed separation. A similar behavior is observed for the area of maximum v' values, where it is also shifted towards the downstream side of the aperture. Figures 6(b), 6(d) and 6(f), indicate that there is change in the wake area. The turbulence intensity of the v-component presents a reduction in its maximum value of 20% for the modulated sine wave and 15% for the pure sine wave when compared to the baseline case shown in figure 6(b).

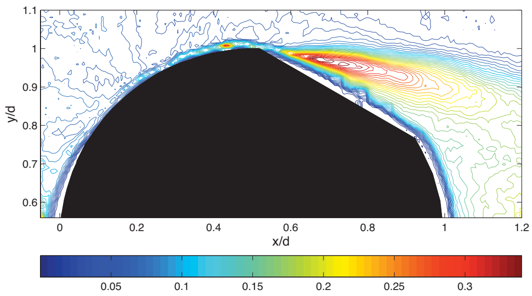

(a) u'/U_∞, Baseline, no control

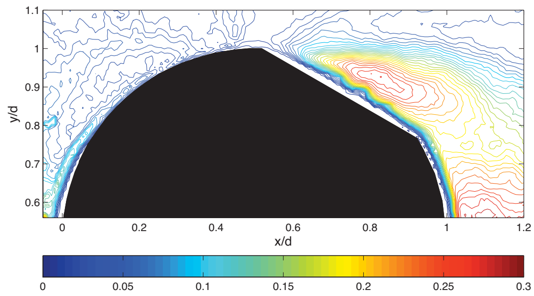

(b) v'/U_∞, Baseline, no control

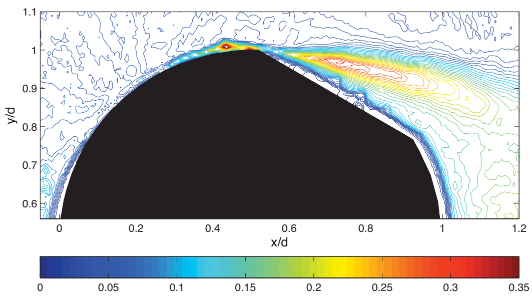

(c) u'/U_∞, MSW, $f^+ = 1$

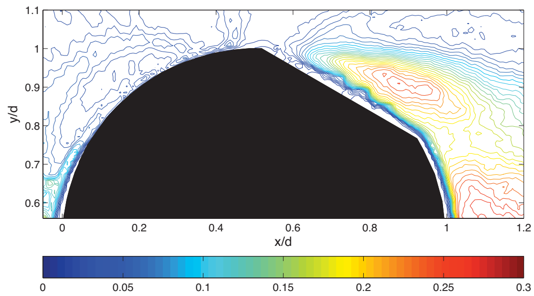

(d) v'/U_∞, MSW, $f^+ = 1$

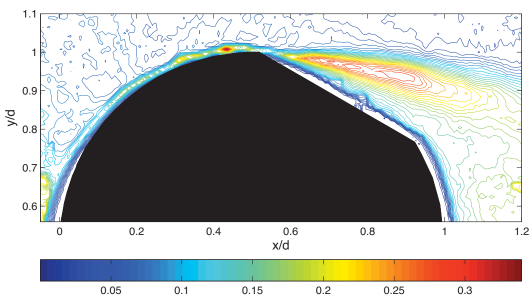

(e) u'/U_∞, PSW, $f^+ = 8$

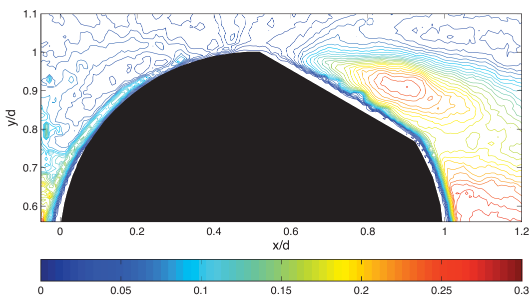

(f) v'/U_∞, PSW, $f^+ = 8$

Figure 6. Normalized turbulence intensities for baseline, modulated sine wave and pure sine wave, where a, c, and e present u'/U_∞ and b, d and f present v'/U_∞

Figure 7 presents a comparison of the normalized Reynolds shear stress for baseline and the two open-loop control cases. The baseline case presents a range from 0.02 to 0.06 over most of the aperture. Its maximum level of 0.06 is located over the center of the aperture. A clear reduction of the shear stress of 28% can be observed between the baseline and both actuated cases, shown in figures 7(b) and 7(c). Another interesting feature, as we compare the actuated cases with the baseline case, is that the location of the maximum Reynolds shear stress is shifted towards the downstream side of the aperture for both actuated cases. This can indicate that the separation is being delayed. The reduction of both turbulence intensities and shear stress are of the same order, as expected, which indicates a reduction of the separation.

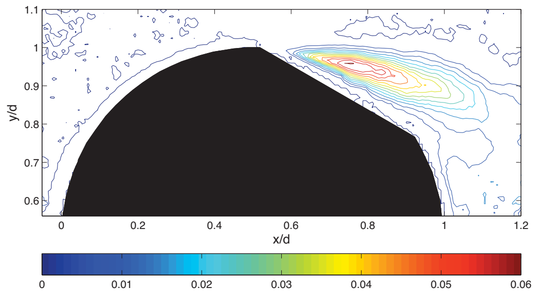

(a) Baseline, actuation OFF.

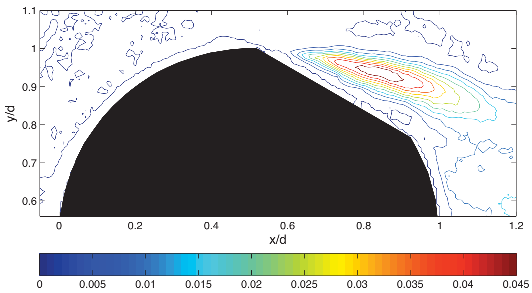

(b) Modulated sine wave, $f^+ = 1$

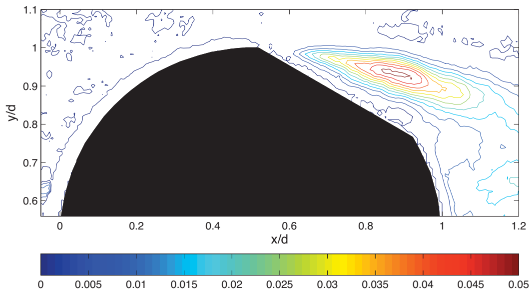

(c) Simple sine wave, $f^+ = 8$

Figure 7. Normalized Reynolds <–uv> shear stress.

B. Unsteady surface pressure measurements

There is an interest in the unsteady surface pressure measurements for the purpose of control. From the controls point of view, we would like to use practical measurements to sense the flow conditions and in the future relate this with the optical conditions in real-time to then act upon it. The time-resolved fluctuating pressure signals were acquired in sets that cover about 70 seconds. These were then divided into blocks of .25 seconds to consider each block as a statistically independent realization. Each set provided about 280 blocks and allowed us to make averages of the two-point in time statistics. When we look at the time series, figures 8(b) and 8(c), of the actuated cases we no longer see large fluctuations on the range –0.4 to 0.5 that occurred for the baseline case (figure 8(a)), basically the fluctuations stay between –0.2 and 0.2. Table 2 presents the statistics for the three cases studied. These results present an increase of the rms in each of the actuated cases. At first this seems counter intuitive, but considering that the actuation has a velocity ratio of 1.67, a momentum coefficient of $1.7{\times}10^{-3}$ and our velocity results we can conclude that the actuation is increasing the local fluctuations at the surface and reducing the global fluctuations. These results are also in agreement with results presented by Wallace et al. (2010) were a similar test model is used and flow control is performed by applying suction. Interesting to notice that the skewness, s, is changed significantly for the pure sine wave case ($f^+ = 8$) driving the distribution almost to a gaussian. The actuation also reduces the kurtosis, κ, in both actuated cases.

$$\rho(\tau) = \frac{\overline{p(t)p(t+\tau)}}{\overline{p(t)^2}} \tag{3}$$

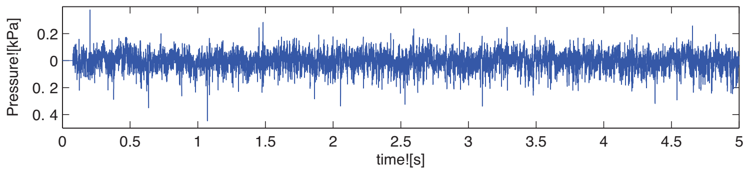

(a) Baseline

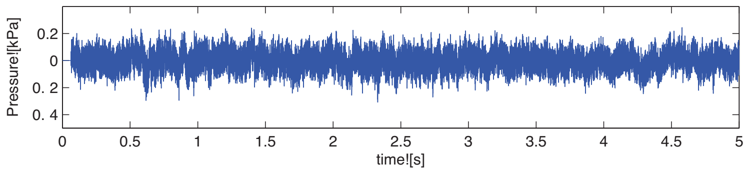

(b) Modulated sine wave, $f^+ = 1$.

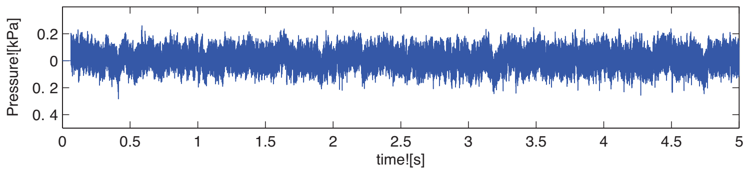

(c) Pure sine wave, $f^+ = 8$.

Figure 8. Pressure time series.

Table 2. Pressure statistics for all studied cases for sensor 3.

case	p' (kPa)	s	κ
Baseline	0.0562	-0.2389	3.959
Modulated sine wave	0.0616	-0.1569	3.002
Pure sine wave	0.0739	-0.0688	2.853

Pressure spectra for all the sensors along the center plane (i.e. sensors 3, 8, 13, 18, 23, and 28) are presented in figure 9, for the cases studied. The shedding frequency around 40 Hz can be observed in all three cases. In the case of modulated sine wave there are peaks at every 100 Hz and for the simple sine wave peaks occur every 200 Hz. The driving frequencies of the actuators, 2.2 and 2.4 kHz are observed for both controlled cases.

A look at the pressure autocorrelations is performed to evaluate the typical integral time scales that are present across the turret's surface. The autocorrelation function was computed using the fluctuating pressure from the same location at two different times, t and t', shown in equation 3. Figure 10(a) shows the autocorrelation for all the sensors over the surface of the turret. We like to observe the overall behavior of the unsteady surface pressure. A broad range of integral time scales can be seen here, that are within the dimensions of the model if one uses Taylor's hypothesis to map time to space. Taylor's hypothesis states that at a given point turbulence advects with mean velocity and can be approximated from a frozen pattern of turbulence. This allows spatial information to be estimated from time resolved data, such as the fluctuating pressure measurements. Note in particular the strong spatial inhomogeneity of these pressure correlations clearly shows the highly three-dimensional nature of the flow. In the baseline we see autocorrelations that are representative of a turbulent flow. The pressure autocorrelations for the actuated cases are shown in figures 10(b) for the modulated sine wave and 10(c) for the pure sine wave, indicate that the actuation changes the flow considerably. When actuation is applied, the autocorrelations exhibit a more organized almost periodic behavior. Organization of the

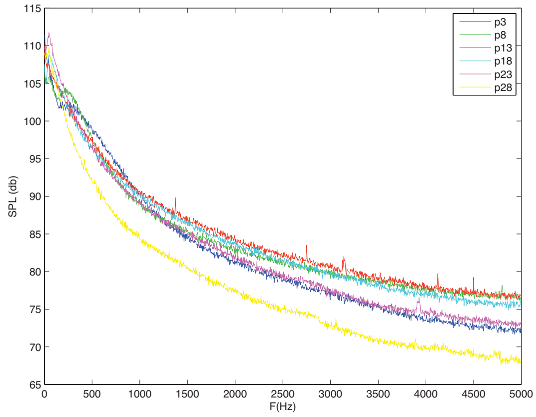

(a) Baseline

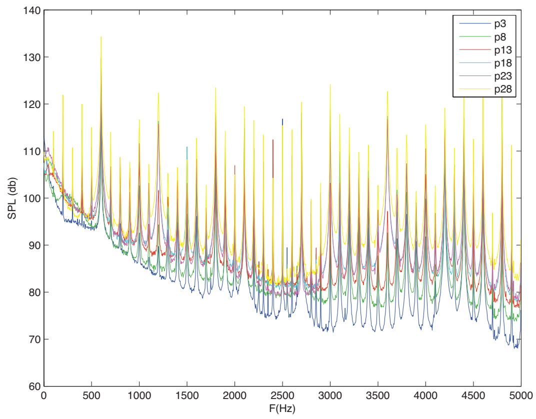

(b) Modulated sine wave, $f^+ = 1$

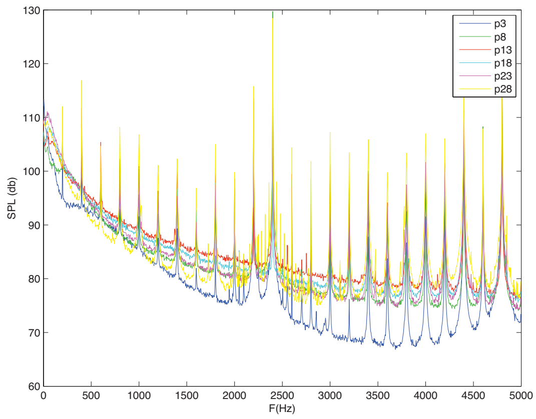

(c) Pure sine wave, $f^+ = 8$

Figure 9. Pressure spectra for sensors at the center plane.

autocorrelations is seen for both types of actuation. This result is encouraging from an adaptive optics point of view as discussed by Jumper et al. (2001) and Fitzgerald et al. (2004). They argue that by using flow control it may be possible to regularize the shear layer simplifying the application of adaptive optics. We notice that the control is able to "regularize" the shear layer at this low Reynolds number. Note that the instantaneous velocity snapshots shown for both control cases in figures 5(b) and 5(c) appear to have a somewhat periodic behavior consistent with the pressure autocorrelations shown in figures 10(b) and 10(c).

IV. CONCLUSIONS AND FUTURE WORK

Experiments on a three-dimensional turret with a flat aperture were performed at Syracuse University. The effects of the flow control were studied by examining the velocity and unsteady surface pressure measurements. The tests were performed at a Mach number of 0.1 corresponding to a Reynolds number of 300; 000. An actuation system containing 22 piezoelectric disks was implemented for flow control purposes. In these tests three cases were studied that included: baseline, modulated sine wave and pure sine wave. Simultaneous wall pressure and velocity measurements were done to capture the behavior of the flow field over the turret model for these three cases and comparisons made between them to quantify the effects of the control.

A reduction of the maximum u' values of 20% is perceived between the baseline and both actuated cases. The area with the maximum turbulence intensity also shifts slightly to towards the downstream side of the aperture, an indication of delayed separation. A similar behavior is observed for the area of maximum v' values, where it is also shifted towards the downstream side of the aperture. The turbulence intensity of the v-component presents a reduction in its maximum value of 20% for the

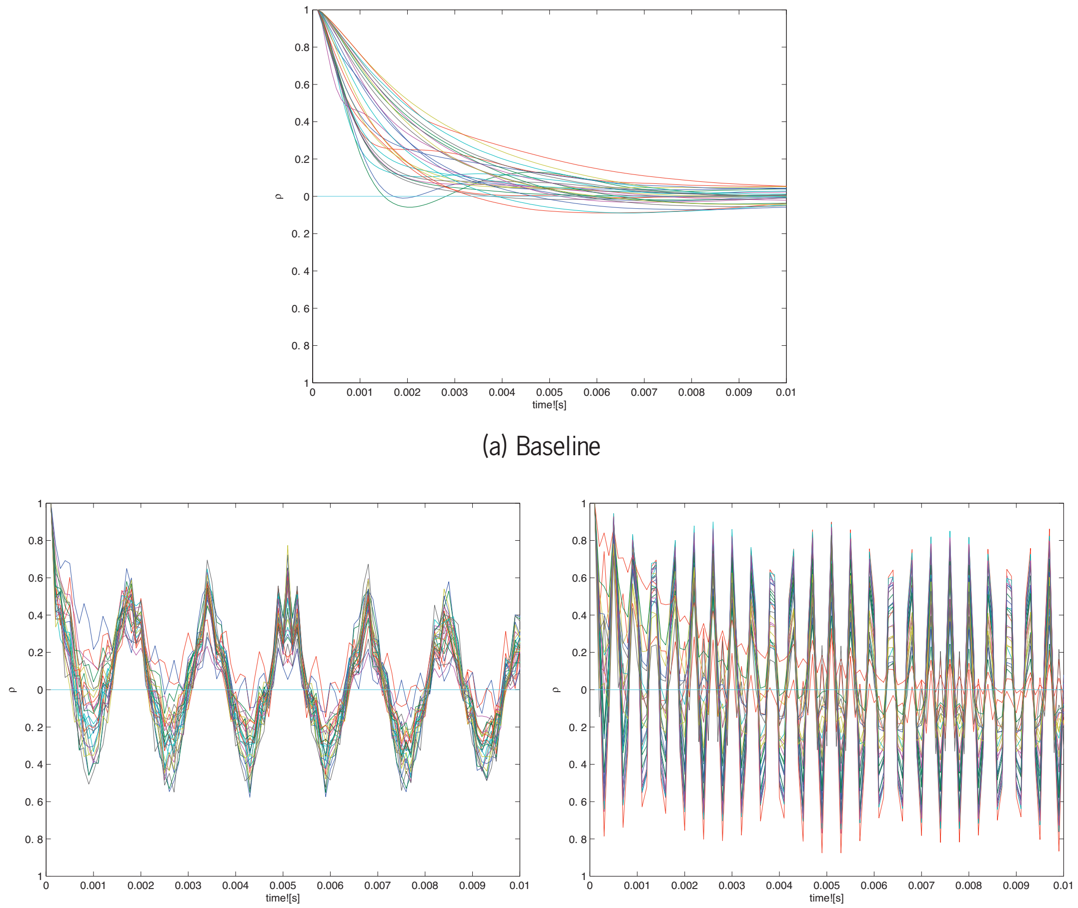

(a) Baseline

(b) Modulated sine wave, $f^+ = 1$

(c) Pure sine wave, $f^+ = 8$

Figure 10. Pressure autocorrelations of all the sensors across the turret's surface for all the cases studied.

modulated sine wave and 15% for the pure sine wave when compared to the baseline case. A comparison of the normalized Reynolds shear stress for baseline with the two open-loop control cases exhibits a reduction of the shear stress of 28% between the baseline and the modulated sine wave case and 10% reduction for the case of pure sine wave. The reduction of the turbulence intensities indicates a reduction of the separation.

The pressure autocorrelations for the baseline, the modulated sine wave and for the pure sine wave, indicate that the actuation changes the flow considerably. In the baseline we saw autocorrelations that are representative of a turbulent flow, as discussed earlier. When actuation is applied, the autocorrelations exhibit a more organized almost periodic behavior. Organization of the autocorrelations is seen for both types of actuation. This result is encouraging from an adaptive optics point of view as discussed by Jumper et al. (2001) and Fitzgerald et al. (2004). They argue that by using flow control it may be possible to organize the shear layer simplifying the application of adaptive optics. We notice that the control is able to "organize" the shear layer at these lower Reynolds and Mach numbers. Note that the instantaneous velocity snapshots shown for both control cases appear to have a somewhat periodic behavior consistent with the pressure autocorrelations.

The results presented here are in good agreement with tests performed by Andino et. al (2010) at a Reynolds number of 2; 000; 000 corresponding to a Mach number of 0.3. The tests were performed using basically the same geometry but with a diameter of 30.48 *cm*. Openloop control was applied showing an increase in the unsteady surface pressure measurements for the simple sine wave and for the f+ = 1. Results at low and high Reynolds number present the same effects on the third and fourth moments of the pressure. We can infer that a reduction on the velocity field fluctuations is expected based on the results obtained at low Reynolds number.

We will continue to analyze the extensive data base obtained. A study of the turbulence production term will be done to evaluate the effect of control. The results presented here suggest that a reduction in the production will occur when the control is applied since the mean gradients are reduced. In addition a POD analysis will be done on the $\tilde{u}$, $\tilde{v}$ velocity with and without control to observe the change in the flow structures due to the control. We are also interested in developing a low dimensional description of the flow field through the use of velocity and unsteady surface pressure measurements. This will incorporate velocity-pressure correlations and mathematical tools such as Proper Orthogonal Decomposition,[13] POD, and Modified Linear Stochastic Measurements,[14] mLSM to construct a low dimensional velocitybased closed-loop flow control model to estimate the flow states in real-time.[15]

REFERENCES

[1]Gilbert, K.G., and Otten, L.J. (Eds.). (1982). Aero-optical phenomena. *Progress in astronautics and aeronautics*, 40, AIAA, New York.

[2]Jumper, E.J., and Fitzgerald, E.J., ”Recent advances in aero-optics”, *Progress in aerospace sciences*, Vol. 37, No. 3, 2001, pp. 229-339.

[3]Fitzgerald, E. J., and Jumper, E. J., (2004). The optical distortion mechanism in a nearly compressible free shear layer. *J. Fluid Mech.*, 215, 153-189.

[4]Gordeyev, S., Hayden, T., and Jumper, E., ”Aero-optical and flow measurements over a flat-windowed turret”, *AIAA Journal*, Vol. 45, No. 2, 2007.

[5]Gordeyev, S., Jumper, E.J., Ng, T., and Cain, A.B., ”The optical environment of a cylindrical turret with a flat window and the impact of passive control devices”, AIAA Paper 2005-4657, June 2005.

[6]Vukasinovic, B., Glezer, A., Gordeyev, S., Jumper, E., and Kibens, V., ”Active control and optical diagnostics of the flow over a hemispherical turret”, AIAA Paper 2008-0598, January 2008.

7Andino, M. Y., Wallace, R. D., Glauser, M. N., Camphouse, R. C., Schmit, R. F., and Myatt, J. H., Boundary feedback flow control: Proportional control with potential application to aero-optics. to appear in *AIAA Journal*, June 2009.

[8]Amitay, M., and Glezer, A., ”Controlled transient of flow reattachment over stalled airfoils”, *Int. J. Heat and Fluid Flow*, Vol. 23, 2002, pp. 690-699.

[9]Smith, D.R., ”Interactions of a synthetic jet with crossflow boundary layer”, *AIAA Journal*, Vol. 40, No. 11, Novemnber 2002, pp. 2277-2288.

[10]Yehoshua, T., and Seifert, A., “Boundary condition effects on oscillatory momentum generators”, AIAA Paper 2003-3710, June 2003.

[11]Woszildo, R., Taubert, L., and Wygnanski, I., ”Manipulating the flow over spherical protuberances in a turbulent boundary layer”, *AIAA Journal*, Vol. 47, No. 2, 2009, pp. 437-450.

[12]Wallace, R. D., Shea, P. R., Glauser, M. N., Vaithianathan, T., and Carlson, H. A., “Feedback flow control for a pitching turret”, AIAA Paper 2010-0361, January 2010.

[13]Lumley, J. L. (1967). The structure of inhomogeneous turbulence. In Yaglom, A. M. & Tatarski, V. I. (Eds.), Atmospheric turbulence and radio wave propagation (pp. 166-178). Nauka, Moscow.

[14]Bonnet, J. P., Cole, D. R., Delville, J., Glasuer, M. N., and Ukeiley, L. S. (1994). Stochastic estimation and proper orthogonal decomposition: Complimentary techniques for idntifying structures. *Experiments in Fluids*, 17 (5), 307-314.

[15]Pinier, J.T., Ausseur, J.M., Glauser, M.N., and Higuchi, H., Proportional Closed-Loop Feedback Control of Flow Separation, *AIAA Journal*, Vol.45, No.1, 2007, pp. 181-190.